



The effect of microchannel-porous media and nanofluid on temperature and performance of CPV system

Somayeh Davoodabadi Farahani¹ · Mahdi Alibeigi¹ · Amir Zakinia¹ · Marjan Goodarzi^{2,3}

Received: 11 May 2021 / Accepted: 18 September 2021 / Published online: 5 October 2021
© Akadémiai Kiadó, Budapest, Hungary 2021

Abstract

This numerical study on the effect of microchannels with porous medium and nanofluid on the solar concentrator photovoltaic (CPV) system with a solar concentration ratio of 10 is presented. Numerical simulation is two-dimensional and different layers of CPV are modeled. The effect of the position of the porous layer in the microchannel on the cooling of the PV system is investigated. The thermal behavior of the microchannel with the porous layer varies with the change of Darcy number, and the porosity coefficient according to the position of the porous layer in the microchannel is studied. The consequences demonstrate that the solar cell temperature is reduced by about 17% using the microchannel. The development of the microchannel cooling capacity is related to the rise in thermal conductivity in the porous layer. Also, in the porous layer cases, located in a block width across the microchannel, the maximum electrical efficiency rate and the minimum of the solar cell temperature occurred. The raising of the nanofluid volume fraction has improved the CPV system's electrical efficiency. Consequently, the solar cell temperature can be reduced from 1 to 52% with the increment of radiation intensity from 100 to 1000 Wm⁻². The proposed cooling method is about 30% more effective than the conventional fin cooling method.

Keywords CPV · Microchannel · Porous media arrangement · Temperature

List of symbols

C	Specified heat capacity, J kg ⁻¹ K ⁻¹
C_p	Specific heat capacity, J kg ⁻¹ K ⁻¹
CR	Solar concentration ratio
d	Diameter, m
H	Diameter of the microchannel, m
k	Thermal conductivity coefficient, Wm ⁻¹ K ⁻¹
L	Length of microchannel, m
m	Mass flowrate, kgs ⁻¹
P	Pressure, kPa
q	Heat flux, Wm ⁻²
T	Temperature, K
U	Inlet velocity, ms ⁻¹
V	Velocity, ms ⁻¹

Dimensionless numbers

Re	Reynolds number
Da	Darcy number

Greek symbols

ρ	Density, kg ⁻³
η	Thermal efficiency
μ	Fluid dynamic viscosity, Pa s
α	Thermal diffusion coefficient, m ² s ⁻¹
\varnothing	Volume fraction
κ	Permeability, m ²
τ	Porous thickness, m
ε	Porosity coefficient
δ	Thickness, m

Subscripts

abs	Absorbed solar radiation
amb	Ambient
bf	Working fluid
c	Coolant
cell	Cell
dr	Drift
el	Electrical
f	Fluid
in	Inlet
mi	Mixture

✉ Marjan Goodarzi
mgoodarzi@lamar.edu

¹ School of Mechanical Engineering, Arak University of Technology, 38181-41167 Arak, Iran

² Department of Medical Research, China Medical University Hospital, China Medical University, Taichung, Taiwan

³ Department of Mathematics, Faculty of Science, King Abdulaziz University, P.O. Box 80259, Jeddah, Saudi Arabia

out	Outlet
p	Particle
r	Standard conditions
ref	Reference
s	Solid
th	Thermal
w	Wind

Introduction

The photovoltaic thermal (PV/T) is an energy conversion system that can directly convert solar radiation energy into electrical energy. However, the received solar radiant energy cannot be converted into electrical energy completely by the PV/T system, and the remaining part changes to heat. This point is the cause of this system's low efficiency (4–17%), which increases the temperature of photovoltaic cells [1, 2]. In addition, due to the open-circuit voltage, reductions in system efficiency occurred [3]. Also, increasing the temperature of photovoltaic (PV) cells damages the system's structure and reduces its useful life. Accordingly, it can be reduced to some extent. These systems are also called thermal photovoltaic systems. Thermal photovoltaic systems are a combination of conventional photovoltaic systems and heat collectors for the simultaneous production of electrical and thermal energy. Simultaneous use of electrical and thermal units reduces the occupied space, reduces the temperature of cells, and thus increases the life of the system and also increases the overall efficiency (electrical and thermal) of the system. Another way to cool a PVT system is to add a backside to it. As a result, the heat generated by the solar panel is dissipated. In this case, the system operates at a lower temperature, and its efficiency is higher [4, 5].

Another technique suggested by researchers for cooling the PVT system is the use of a cooling fluid. Daghigh et al. [6] examined in a review article the performance of thermal photovoltaic systems with different operating fluids such as pure water, refrigerant, and mixing water with air in a two-phase model (air/water mixture). Moghadammi et al. [7] reported that by using nanofluids at high velocities and high volume fractions of nanofluid, the efficiency of the solar panel increases by about 76%. Bhatarai et al. [8] deliberated water as the base fluid for discovering the performance of the PV/T-system which is associated with a solar collector. They evidenced that the PV/T-system efficiencies and the solar collector efficiencies are 70.58 and 50.71%, respectively. They also computed that the PV/T-system electrical efficiency is 69.13%. Hazami et al. [9] investigated electricity supplying and hot water for domestic consumption with numerical and experimental methods in the PV/T-system performance. The maximum thermal efficiencies have been computed, and the electrical of the PV/T-system is 50 and

15%, respectively. Yazdanifard et al. [10] numerically investigated the laminar and turbulent flow efficacy in a PV/T-system with water working fluid. They also deliberated the Reynolds number, length of the collector, solar radiation intensity, coating, the collector tube diameter, and the number of the collector tubes efficacies on the PV/T-system performance. Their study delivered that the system efficiency in turbulent flow is more than in laminar flow.

Similarly, they concluded that increasing solar radiation increases the efficiency of the system. In the nanofluids, The metal nanoparticles' dispersion is the cause of the thermal conductivity coefficient rising in the working fluid [11]. Therefore, in a PV/T-system, the nanofluid usage as an operating fluid can be an operative way to increase the system efficiency. Notably, the nanofluids application in a PV/T-system is associated with some restrictions, for example nanoparticle's high price, instability of nanofluids, and the pressure drop increasing in nanofluids [12, 13]. Lately, studies have been conducted to examine the impacts of applying several nanofluids on the PV/T-systems performance. Taheri et al. [14] premeditated the effectiveness variable performance parameters on the (PV/T) with the working fluid of water. They concluded that growth of the cell efficiency, coverage coefficient, mass of water-to-collector surface ratio, and wind speed increases system performance without glass coating. While increasing sunlight and ambient temperature have the most significant effect on the glass-covered system. Also, using a carbon–water nanotube mixture, PVT's energy efficiency, and exergy increase by about 12% and 1.23%, respectively. Dehghan et al. [15] experimentally intended at revealing the techno-economic analyses of the temperature management of photovoltaic (PV) modules with two different cooling situations consists of case A and Case B with 3 and 6 low-energy fans per module, respectively.

Al-Shamani et al. [16] studied the influences of nanofluids of silicon oxide/water, titanium oxide/water, and silicon carbide/water on the PV/T-system performance. They detected that the nanofluid of silicon carbide as a working fluid has the most efficient than the others. Correspondingly, the electrical and overall system efficiencies with silicon carbide nanofluid as working fluid were calculated at 52.13 and 73.81%, respectively. Alshaheen et al. [17], in an experimental investigation, explored the performance of PV/T-system with an operating fluid of carbon-based nanofillers/ water. They also evaluated the effect of and nanoparticle volume fraction and flow Reynolds number on system performance. They concluded that energy efficiency and exergy increased by about 12 and 1.43% at a volume fraction of 0.05, respectively. In a numerical investigation, Rajab et al. [18] investigated the using aluminum oxide and copper nanoparticles efficacy with a volume fraction of 1.0, 2.0, and 4.0% on the PV-system thermal. Their conclusion disclosed that water as the base fluid enhances the efficiency of the system rather

than ethylene glycol. They also settled that the maximum electrical and thermal efficiency against the others occurred when the nanofluid of the system was nanofluid of Cu/water with a volume fraction of 4.0%. Sardarabadi et al. [19] inspected experimentally and numerically the PV/T-system performance with nanofluids such as titanium oxide–water, zinc oxide water, and aluminum oxide–water in the volume fraction of 2.0%. Their study showed that systems with titanium oxide–water, and zinc oxide–water nanofluids have the highest electrical efficiency. They also observed that the system with zinc oxide–water nanofluids has the highest thermal efficiency. Sharma et al. [20] examined the enhancement of the PV/T-system performance by applying a phase change material (PCM) with nanoparticles. They found that the maximum temperature of the photovoltaic (PV) cell was reduced by about 15 and 18.5% with PCM and the PCM-nanoparticle, respectively. Dehghan et al. [21] numerically studied on a 3-D conjugate heat transfer of Al_2O_3 –water nanofluid through rectangular microchannel heat sinks (MCHS). They reported when the thermophysical properties of fluid is temperature dependent, the simulation results are more realistic, particularly for converging flow passages due to high-temperature gradients and for nanofluids for their induced temperature-dependent properties. In another study, Dehghan et al. [22] investigated the converging flow passages on the forced convection heat transfer coefficient in a MCHS by using nanoparticle (Al_2O_3). They analytically solved porous media inside microchannels in the slip regime, based on the local thermal nonequilibrium model with two-phase model. Their result showed that the convection heat transfer coefficient in the converging flow passages is 33% higher than that of straight passages.

Using numerical simulations, Rabie et al. [23] investigated the thermal photovoltaic system using phase-change materials. They distinguished that the maximum cell temperature was reduced from 92 to 74 °C. Siyabi et al. [24] studied the actions of a high-concentration photovoltaic solar cell segment connected to a multilayer microchannel heat tank. They found that when a three-layer microchannel was used, the electrical efficiency enriched by about 10%, and the maximum cell temperature decreased by about 70%. Abo-Zahhadet al. [25] numerically studied the usage of microchannels in PV/T-system. They detected that by varying the coolant flow rate in the range of 25 to 1000 g min^{-1} . As a result, the maximum temperature of the photovoltaic (PV) cell reaches in range of 71.7–40.1 °C. They also discovered that the geometry of the channel has a significant impact on system performance.

In some studies, the energy storage potential of phase change materials has been used to cool the PVT system [26–28]. The use of phase change materials improves the efficiency of the PV system by about 15%. For example, Nasef et al. [29] explored using the phase change material

(PCM) and the nanofluid in the PV-system performance. They identified that the reduction of cell temperature was almost 60 and a 15% intensification in system efficiency.

A review of previous studies shows that solutions and suggestions for cooling photovoltaic systems have been presented numerically and experimentally based on the heat sink [30, 31], heat sink-microchannels [32, 33], nanofluids [34, 35], and phase change material [36, 37]. Few studies have been performed on the performance of porous media as photovoltaic cooling heating systems, and the lack of knowledge in this area is strongly felt. In this exploration, the impacts of using a microchannel with a porous layer and nanofluid on the temperature distribution and electrical efficiency of the photovoltaic (PV) system are examined. According to the parameters consist of porosity coefficient, nanoparticle volume fraction, Darcy number, and positional porous layer efficacy on the PV-system performance is inspected. The effect of the position of the porous layer in the microchannel on the cooling of the PV system is investigated. The finite volume method is used for numerical simulation, and nanofluid modeling is considered a two-phase flow.

Problem description

The present numerical investigation is intended to use microchannel-porous media on the solar concentrator photovoltaic (CPV) system with solar concentration ratio (CR) of 10. A 2-D (division) diagram of the problem is demonstrated in Fig. 1. Three components of the Fresnel lens solar cell are considered. The proposed PV concentrator system with microchannel (CPV-micro) includes three complimentary same Fresnel lens, encapsulation sheet, aluminum backplate, three same silicon solar cells [38], and optional microchannel. At the top of the system, the whole Fresnel lens are located. All the solar cell thickness is measured in 1 mm, set at the parallel of a Fresnel lens photosensitive axis. Typically, it is positioned along with the concentration ratio of the base system with an amount of 10 and principal lens length. Encapsulating components are applied to cover all solar cell borders to control the sun rays emission with a thickness of 1 mm [39]. To set a cooling system, a microchannel is installed at the bellow of the PV concentrator with investigating the positional porous layer effect in the microchannel on the CPV cooling system performance. Nearby the high-bounded wall of the microchannel and the lowest-bounded wall is isolated. The microchannel length is L , and the microchannel height is H .

A simple microchannel without a porous layer is considered. Also, the porous material is aluminum. First of all, in case 1, porous layer has been placed by two individual equal thickness τ walls, located upper wall of the microchannel

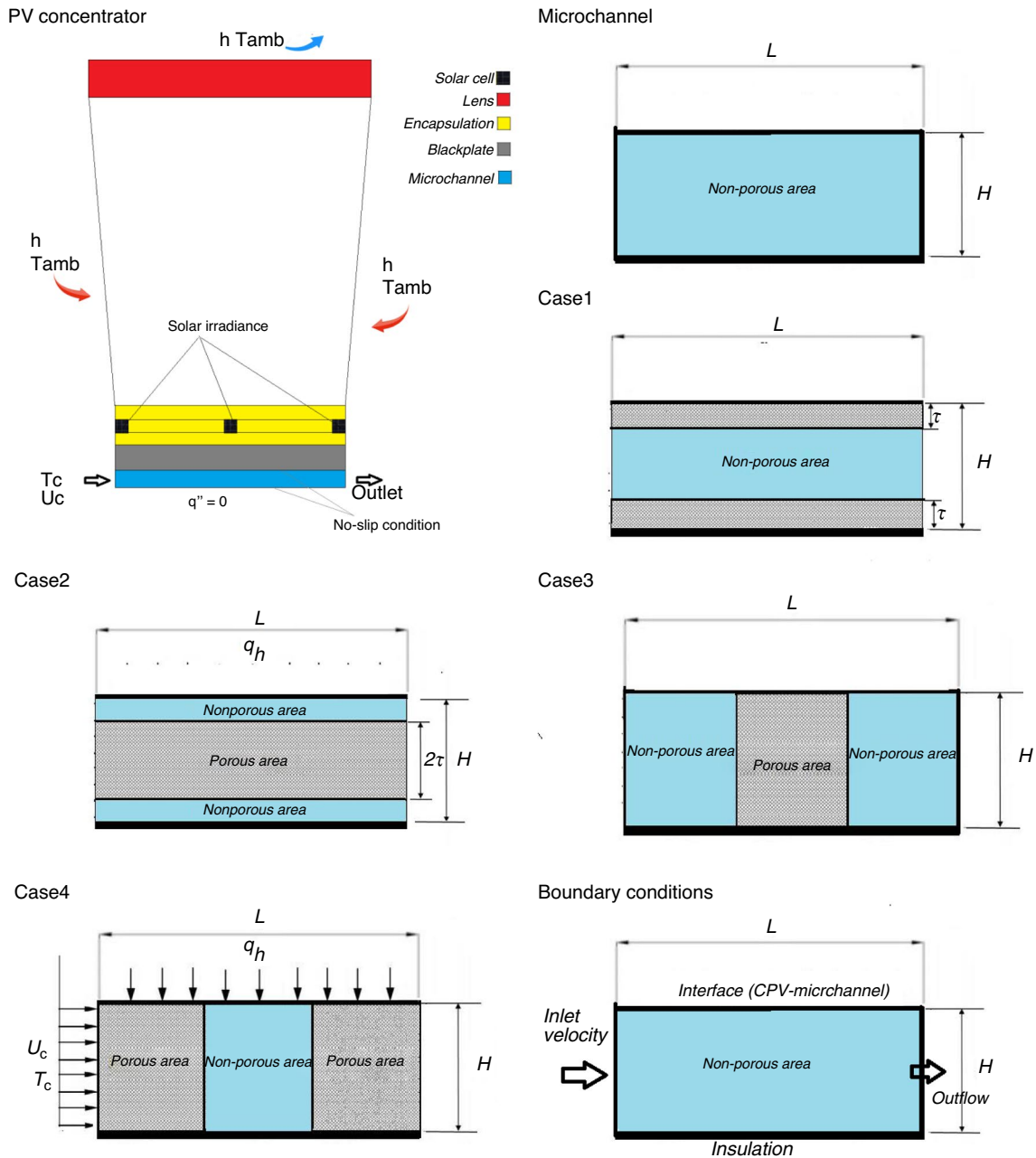


Fig. 1 Schematic of the CPV system with microchannel and the position of the porous layer

and the down wall of the microchannel. The rest is the non-porous layer. Moreover, in case 2, the porous layer has been chosen with one wall with thickness 2τ in the middle of the microchannel, and the two-rest layer is nonporous. Also, the microchannel has separated into three-divided areas in the porous plane layer. Put the porous layer in the middle section in case 3, and put two-divided porous plane layer in the left and right sides of the microchannel in case 4 has been proposed [40]. Comparison of porous and nonporous microchannel aids to choose the best mod of the system installation. In these four cases for the location of the porous

layer has been considered. All the cases which have been discussed earlier are specified in Fig. 1.

The cooling fluid in the microchannel is water, and the aluminum oxide nanoparticles are intended for the nanofluid state. The thermophysical properties of each component and the thickness of different parts of the numerical model are expressed in Table 1, respectively. In Table 1, C_p is the specific heat capacity of each component, δ is the thickness of each element, ρ is the density of each element, and k is the thermal conductivity of each component. The thermodynamic properties of various parts of a CPV system are constant. The ohmic

Table 1 Geometric parameters and Thermophysical properties for each component [39]

Component	δ/mm	$\rho/\text{kg m}^{-3}$	$k/\text{W m}^{-1}\text{K}^{-1}$	$C_p/\text{J}/(\text{kg K})^{-1}$	Material
Solar cell	1	2330	148	712	Silicon
Fresnel lens piece	3	1162	0.1875	1465	Acrylic (PMMA)
Backplate	10	2702	238	903	Aluminum
Encapsulation	1	1030	0.16	1100	Sylgard

losses of the system are ignored. Assuming an incompressible, laminar, steady-state fluid flow, the equation of energy, momentum, and continuity for the microchannel is as follows [40]:

$$\rho V \cdot \nabla V = -\nabla P + \mu \nabla^2 V \tag{1}$$

$$V \cdot \nabla T = \alpha \nabla^2 T \tag{2}$$

$$\nabla \cdot V = 0 \tag{3}$$

where V, T, ρ, μ, α and P are velocity, temperature, fluid density, fluid dynamic viscosity, thermal diffusion coefficient, and pressure, respectively. Thermal equilibrium of the porous layer, the continuity of the porous layer, the momentum of the porous layer, and energy equations change of the porous layer are assumed, which can be demonstrated as follows [41]:

$$\vec{\nabla} \cdot (\epsilon \rho_f \vec{V}) = 0 \tag{4}$$

$$\rho_f (\vec{V} \cdot \nabla \vec{V}) = \epsilon^2 \left(\vec{\nabla} P - \left(\frac{\mu_f}{\kappa} + \frac{\rho_f C}{\sqrt{\kappa}} |\vec{V}| \right) \vec{V} \vec{V} + \frac{\mu_f}{\epsilon} \nabla^2 \vec{V} \right) \tag{5}$$

$$\left(\rho_f C_f + \frac{1-\epsilon}{\epsilon} \rho_s C_s \right) (\vec{V} \cdot \vec{\nabla} T) = \left(k_f + \frac{1-\epsilon}{\epsilon} k_s \right) \nabla^2 T \tag{6}$$

where $V, \epsilon, \rho_s, \rho_f, \mu_f, C_s, C_f, P, \kappa, k_f, k_s$ and T are velocity, porosity coefficient, solid density, fluid density, dynamic viscosity, solid specified heat capacity, fluid specified heat capacity, pressure, permeability coefficient, fluid thermal conductivity coefficient, solid thermal conductivity coefficient, and temperature, respectively. The permeability parameter of a porous material, κ , which indicates the ability to transfer or conduct fluid through a porous medium, is defined as follows [41]:

$$\kappa = \frac{\epsilon d_p}{150(1-\epsilon)} \tag{7}$$

where d_p is the diameter of the particles in porous media. The Darcy number is also defined as follows [41]:

$$\text{Da} = \frac{\kappa}{H} \tag{8}$$

where H is the diameter of the microchannel [40, 42]. The base fluid is considered as a two-phase fluid, so the mixture model is employed for modeling. The two phases of the fluid or particles were modeled by solving the equations of continuity, momentum, energy, and volume fraction of the second phase and considering the relative velocity of zero or nonzero between the two phases. In this model, it is assumed that the phases are in continuous environments which, means each phase has within each control volume (CV) there is a volume fraction of the primary phase and a volume fraction of the secondary phase, as well for each phase has an individual velocity vector. The equations of continuity, momentum, energy, and volume fraction are expressed as follows:

$$\nabla \cdot (\rho_{mi} \vec{V}_{mi}) = 0 \tag{9}$$

$$\nabla \cdot (\rho_{mi} \vec{V}_{mi} \vec{V}_{mi}) = -\nabla P + \nabla \cdot (\mu_{mi} \nabla \vec{V}_{mi}) + \nabla \cdot (\emptyset \rho_p \nabla \vec{V}_{dr,P} \nabla \vec{V}_{dr,P}) \tag{10}$$

$$\nabla \cdot \left[\left(\emptyset \rho_p c_{p,P} \vec{V}_P + (1-\emptyset) \rho_f c_{p,f} \vec{V}_f \right) T \right] = \nabla \cdot (k_{mi} \nabla T) \tag{11}$$

$$\nabla \cdot (\emptyset \rho_p \vec{V}_{mi}) = -\nabla \cdot (\emptyset \rho_p \vec{V}_{dr,P}) \tag{12}$$

where \emptyset is the volume fraction. Subscripts of P, mi and f represent nanoparticles, mixtures, and fluids, respectively. \vec{V} and $\vec{V}_{dr,P}$ are the average mass velocity and drift velocity, respectively, which are calculated from the following equations [43]:

$$\rho_{mi} \vec{V}_{mi} = \emptyset \rho_p \vec{V}_p + (1-\emptyset) \rho_f \vec{V}_f \tag{13}$$

$$\vec{V}_{dr,P} = \vec{V}_p - \vec{V}_f \tag{14}$$

The fluid and nanoparticle thermophysical properties are classified in Table 2.

Boundary conditions on the sides and top of the backplate and lens are calculated based on the wind speed (V_w) in the environment and as [39]:

$$q = (2 + 3.8V_w)(T - T_{amb}) \tag{15}$$

where T_{amb} is the environment temperature. The boundary conditions on the microchannel are illustrated in Fig. 1. The

Table 2 Nanoparticle and fluid thermophysical properties [44]

Properties	Unit	Base fluid (Water)	Nano-particle (Alumina)
ρ	kgm^{-3}	995.1	3600
C_p	$\text{J kg}^{-1}\text{K}^{-1}$	4178	765
μ	Pa.s	0.001	–
k	$\text{Wm}^{-1}\text{K}^{-1}$	0.620	36

boundary condition of the upper walls and lower walls of the microchannel has been considered as non-slip conditions. The bottom wall of the microchannel is insulated. The upper wall is the interface between the microchannel and the CPV. Heat is transferred from the CPV system to the microchannel. The coolant enters the microchannel with velocity (U_c) and temperature (T_c). Also, the outflow boundary condition in the microchannel is applied at the outlet microchannel. For cases where a porous medium is used, the following boundary condition is used at the boundary between the porous and nonporous region [45]:

$$\frac{\mu}{\varepsilon} \frac{\partial u}{\partial \zeta} \Big|_{\text{porous zone}} - \mu \frac{\partial u}{\partial \zeta} \Big|_{\text{non-porous zone}} = \zeta \frac{\mu}{\sqrt{\kappa}} u \Big|_{\text{interface}} \quad (16)$$

where ζ and ζ are directions perpendicular to the interface and an adjustable coefficient that accounts for the stress jump at the interface. The Reynolds number is defined in terms of the microchannel diameter and coolant as follows [46]:

$$\text{Re} = \frac{\rho_{\text{bf}} U_c H}{\mu_{\text{bf}}} \quad (17)$$

where ρ_{bf} is the base-fluid density and μ_{bf} is the base fluid's viscosity. The efficiency of PV modules depends on the types of PVs. Baig et al. [47] reported that the rate of decline in PV efficiency is about 0.3–0.5% per degree Celsius increase in temperature. Al-Showany study [48] also examined the electrical efficiency of several PV models and proposed different models for efficiency. In general, for all PVs, the slope of efficiency variation in terms of temperature is 0.45%. In the present study, The PV/T electrical efficiency is presented using an experimental equation calculated by Evans and numerical calculation by Farahani et al. [49, 50]:

$$\eta_{\text{el-r}} = \frac{\eta_{\text{el}}}{\eta_r} = 1 - 0.0045(T_{\text{cell}} - T_{\text{ref}}) \quad (18)$$

where η_{el} , η_r , T_{cell} and T_{ref} are electrical efficiency, electrical efficiency under standard conditions, solar cell temperature, and ambient temperature. Also, for cooling the CPV and

microchannel system, the thermal efficiency is defined as follows [46, 51]:

$$\eta_{\text{th}} = \frac{m_f C_{p,f} (T_{f,\text{out}} - T_{f,\text{in}})}{q_{\text{abs}}} \quad (19)$$

where m_f , $C_{p,f}$, $T_{f,\text{out}}$, $T_{f,\text{in}}$ and q_{abs} are coolant mass flow rate, specific heat capacity, out fluid temperature, inlet fluid temperature, and absorbed solar radiation heat flux.

Grid independence study and Validation

In this investigation, the performance of the CPV system is inspected by the SIMPLE algorithm based on the finite volume method (FVM) with commercial FVM software named ANSYS FLUENT. To investigate the convergence of the solution, the residual values for the continuity equation, velocities in the coordinate axis directions, and the energy equation were selected 10^{-5} , 10^{-6} , and 10^{-8} , respectively.

Grid independence is checked to achieve a more accurate solution. For this purpose, grids with different nodes number have been considered for the CPV system without a microchannel. Solar cell temperature for the total number of nodes 800, 2100, and 2800 was 63, 60.98 °C, and 60.7 °C, respectively. Consequently, the grid with a whole number of 2100 nodes is selected, shown in Fig. 2a. For the CPV system with microchannel, solar cell temperatures for the total nodes of 1630, 3440, and 3950 were 36.1, 35.01, and 34.9 °C, respectively. Finally, the grid with a whole number of 3440 is selected. Grid independence is performed for all cases expressed in Fig. 1. The amount of absorbed solar radiation intensity is equal to 800 Wm^{-2} , the wind velocity in the environment is 1 ms^{-1} , and the ambient temperature is 25°C. Uniform heat flux is considered due to the high uniformity of Fresnel lenses. Due to the high uniformity of the Fresnel lens, the intensity of the sun's radiation is assumed to be uniform. Therefore, uniform heat flux is considered on the cell. In this study, the aim is to investigate the solar cell temperature in different intensities of radiation.

To verify the numerical simulation results, the changes of the solar cell temperature to absorb heat flux in the current study are compared with Natarajan's results [39] and are shown in Fig. 2b. In this case, the CPV system is without the microchannel. The difference between the results is between 1 and 6%. This slight difference indicates the excellent accuracy of the numerical solution presented in the present study. It is observed that the growth of the solar irradiance intensity is the cause of the solar cell temperature increasing. Also, the solar cell temperature is compared with the experimental results [52], and the results are shown in Table 3. The difference between the results is between 6 and 10.89%, indicating good accuracy of the results.

Fig. 2 a Mesh of the case study, b Validation of results for the CPV system

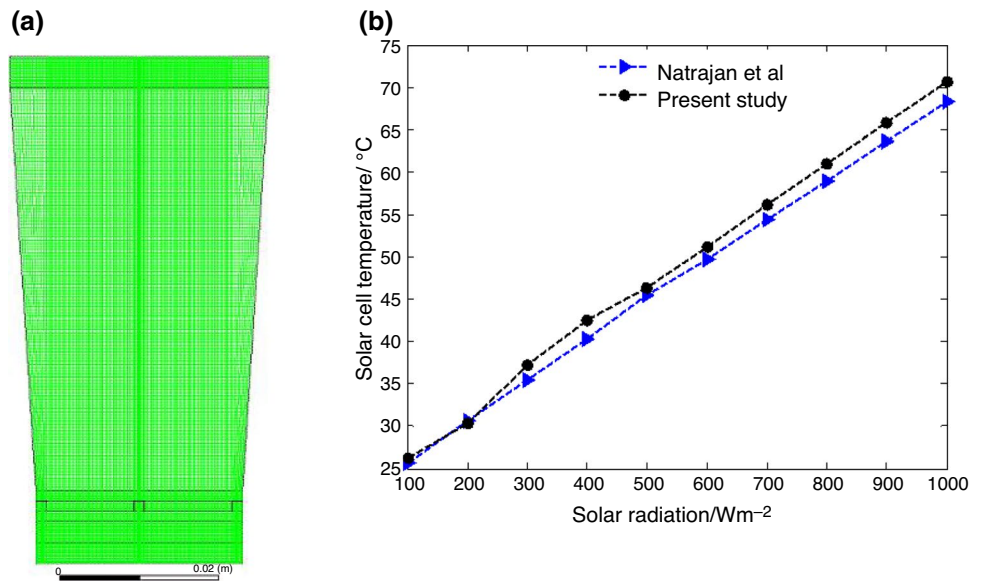


Table 3 Comparison of solar cell temperature in terms of solar radiation intensity

Solar radiation/ Wm^{-2}	Solar cell temperature – ambient temperature/ $^{\circ}C$		Difference/%
	Due et al. [52]	Present study	
750	33.6	30.12	11.55
900	35.6	38.36	7.19
1000	40	47.34	15.50

Results and discussion

Using the proposed modeling, the effects of microchannel application, the position of the porous layer, and the impacts of adding nanoparticles on the CPV system electrical efficiency and the temperature of the solar cell are investigated. Solar cell temperature changes in terms of (a) solar radiation at $Re = 100$ and (b) Reynolds number for CPV and microchannel are illustrated in Fig. 3. The consequences of the solar cell temperature expressed that the CPV and microchannel system is almost 26% less than the CPV system on the surface of solar cell temperature. Also, the Reynolds number from 100 to 1000 change solar cell temperature by nearly $0.2^{\circ}C$ dropped, and this temperature change is low.

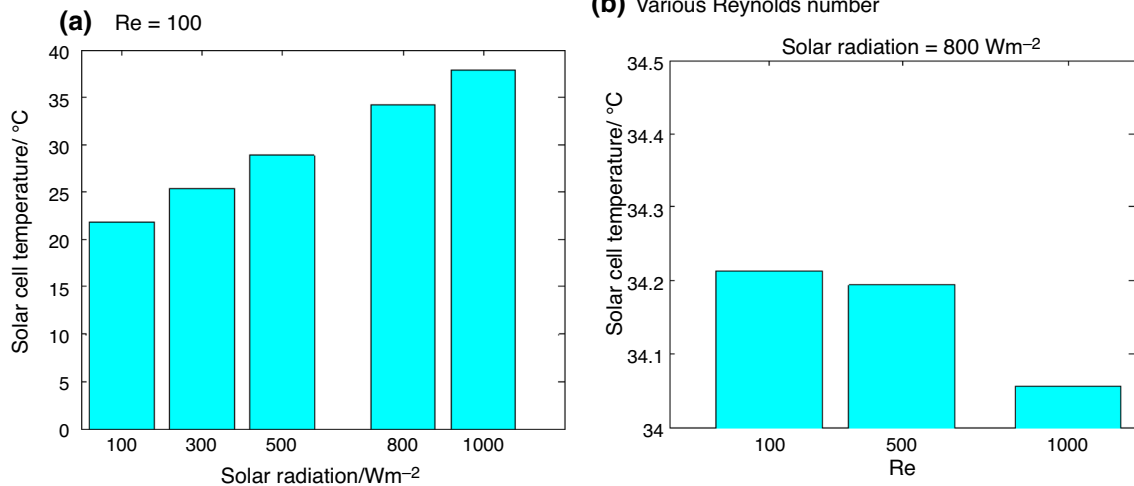


Fig. 3 Solar cell temperature changes

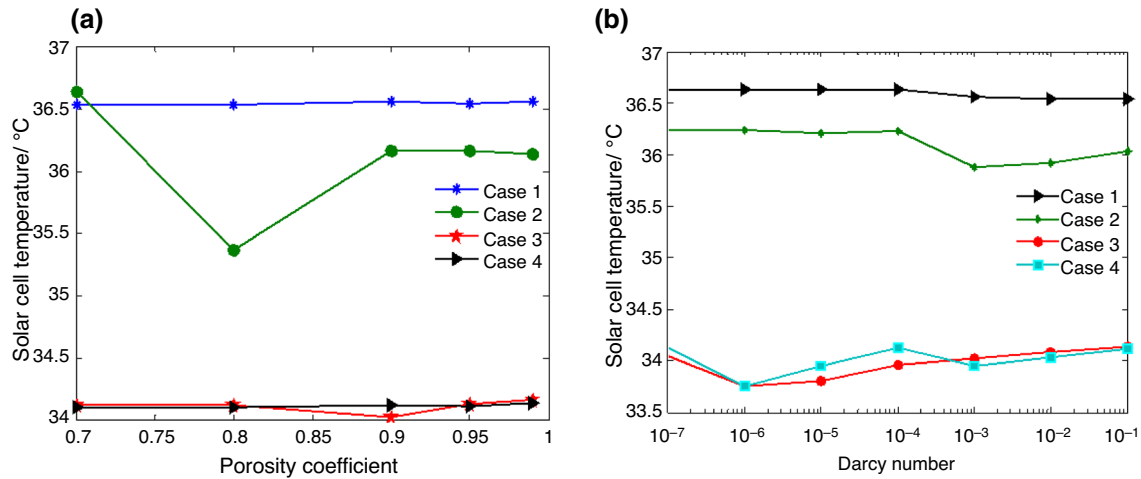


Fig. 4 Solar cell temperature changes

In this section, the CPV and microchannel system with the porous layers is investigated. One of the critical factors in the porous media study always considered is the coefficient of porosity and permeability. Figure 4 illustrates solar cell temperature changes in porosity coefficient and Darcy number for cases CPV and microchannel with the porous layer. When a microchannel with a porous medium is applied, the solar cell temperature decreases rather than the microchannel without a porous medium.

The solar cells' temperature is reduced more when the porous layer is blocked across the channel (cases 3 and 4) than when the porous layer is along the channel (cases 1 and 2). Placing the porous layer across the microchannel cases 3 and 4 causes the fluid temperature to approach the average temperature and increases the temperature gradient on the channel wall. This increases the ability of the microchannel-porous medium to remove heat from the CPV system. As the porous layer is in the center of the channel, the fluid flows more in the nonporous area. Hence, the velocity gradient, followed by the temperature gradient (Chilton-Colburn analogy), increases the channel wall, and more heat from the solar cell to cooling fluid is transferred. Thus, when the porous layer is in the center of the channel, the solar cell temperature is less than when the porous media is close to the channel walls (case 1). One of the characteristics parameters of a porous medium is the porosity coefficient, which affects the solar cell temperature.

The results show that in cases 1 and 4, changing layer's porosity has little effect on the solar cell temperature, for cases 2 and 3, by increasing the porosity coefficient. First, the solar cell temperature decreases to a minimum, and then the solar cell temperature increases. The critical porosity coefficient for cases 2 and 3 is 0.8 and 0.9, respectively. At this porosity coefficient, the heat that the cooling fluid receives is the maximum amount that minimizes solar cells'

temperature. The effect of Darcy number on the temperature of the solar cell has been investigated. Darcy number indicates fluid permeability in the porous medium. In this case, the value of the porosity coefficient is equal to 0.8. The Darcy number indicates the permeability of the fluid in the porous layer. For the case (i.e., cases 1 and 2) where the porous layer is along the channel, the lowest temperature of the solar cell occurs in $Da = 10^{-3}$. In the case (i.e., cases 3 and 4) where the porous layer is across the channel's width, the lowest temperature occurs at $Da = 10^{-6}$. The impacts of the thermal conductivity ratio in the porous layer on the solar cell temperature at $Re = 100$ for diverse porous layer arrangements are investigated, illustrated in Fig. 5. In all arrangements, the solar cell temperature decreases by about 20% to increase the thermal conductivity ratio in the range of 0.1–1. The conductive heat transfer in the porous section increases to raise the thermal conductivity ratio. Thus, the fluid will dissipate more heat from the solar cell, which is the cause of the solar cell temperature reduction. As the Darcy number increases, the amount of fluid that has penetrated the porous region increases, and the effective thermal conductivity coefficient in the porous region decreases, and the amount of heat absorbed by the cooling fluid decreases. Therefore, as the number of Darcy increases, the temperature of the solar cell increases slightly. Figure 6 shows the temperature contour for different modes for solar radiation = 1000 Wm^{-2} , $Re = 1000$, $Da = 0.001$ and $\epsilon = 0.8$. The free convection by the air trapped between the lens and the encapsulation causes the lens temperature to rise due to the absorbed radiation. The heat transfer in the air is from the warmer section of the solar cell to the colder area, the lens. The sylgard material is considered on the topmost and bottommost of the solar cell, which increases the solar cell temperature. Also, it has low conduction. It should be noted that the rise of solar cell temperature influences the efficiency of the system. Therefore,

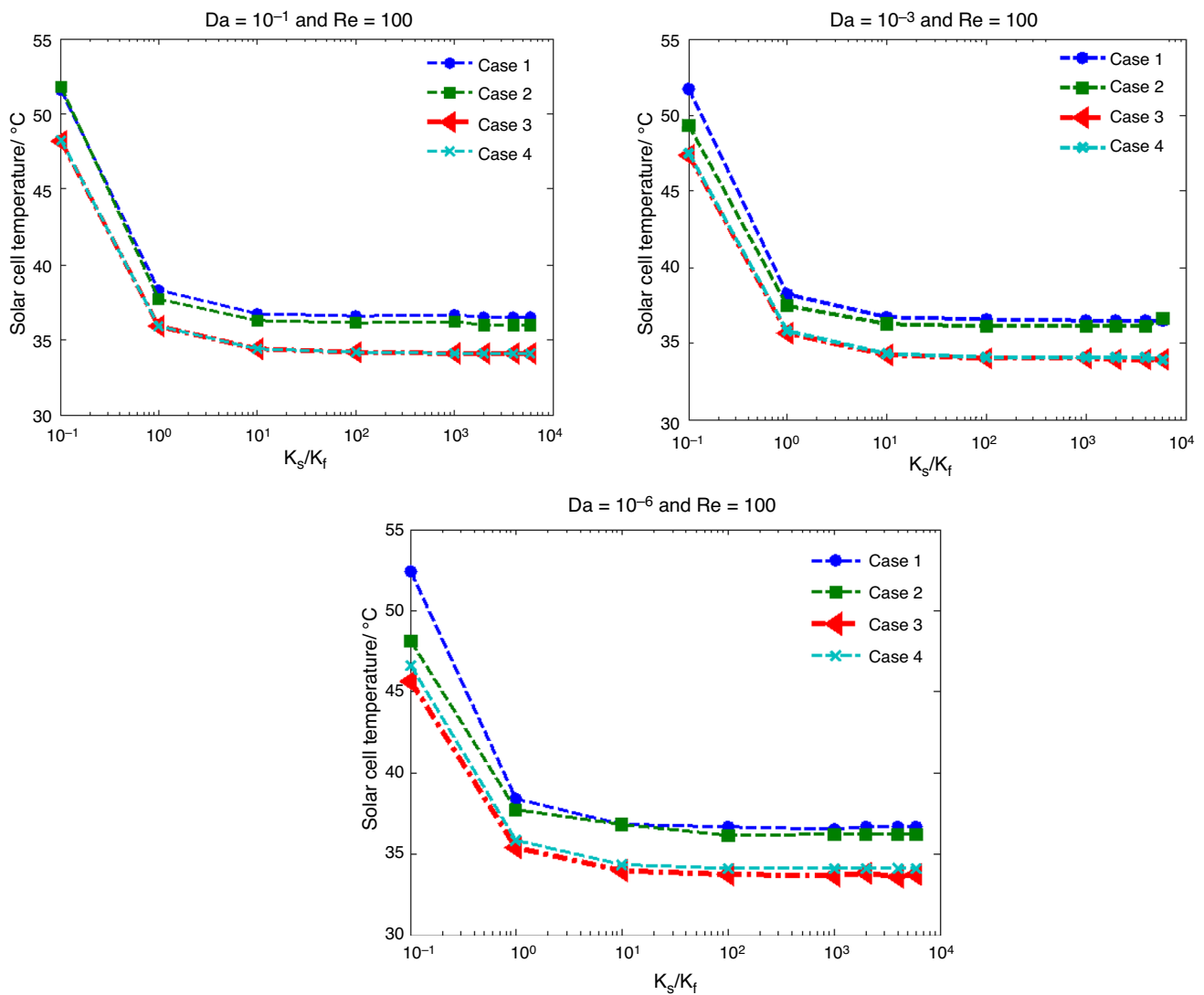


Fig. 5 Solar cell temperature changes according to the thermal conductivity ratio at $Re = 100$

microchannels are applied to reduce the temperature of the solar cell. The contours show that the microchannel-porous media reduced the maximum temperature of the CPV. As a result, the maximum temperature of the solar cell is $31.7\text{ }^\circ\text{C}$. Besides, cases 3 and 4 have the best performance in cooling the CPV system—reducing the CPV electrical efficiency due to increased solar cell temperature. Therefore, the purpose of cooling is to increase electrical efficiency.

The velocity contour for CPV and microchannel modes at $Re = 100, 500,$ and 1000 and four microchannel CPV modes with porous media at $Re = 100$ is shown in Fig. 7. As can be seen, with increasing Reynolds number, the maximum velocity in the channel increases. By placing the porous material in the microchannel, the velocity in the microchannel is reduced. The electrical efficiency ratio variations for different porous layer arrangements are illustrated in Fig. 8.

The behavior of electrical efficiency in terms of porosity coefficient and Darcy number is precisely the opposite of solar cell temperature. In $Da = 10^{-6}, \epsilon = 0.8$, the ratio of electrical efficiency of CPV system of the microchannel with a porous layer in cases 3 and 4 is 0.962 , which is the highest value. The lowest electrical efficiency of the CPV and microchannel system is related to case 1, and this value is equal to 0.948 .

The impacts of the thermal conductivity ratio on the CPV system's electrical efficiency are investigated. The results are exposed in Fig. 9a. With the thermal conductivity ratio growth from 0.1 to 1 , the CPV system electrical efficiency is improved by almost 10% . The electrical efficiency ratios for Case 3 at $\epsilon = 0.8$ and $Da = 10^{-6}$. The thermal conductivity ratios for the three Reynolds numbers $100, 500,$ and 1000 are shown in Fig. 9b. The electrical efficiency ratio for

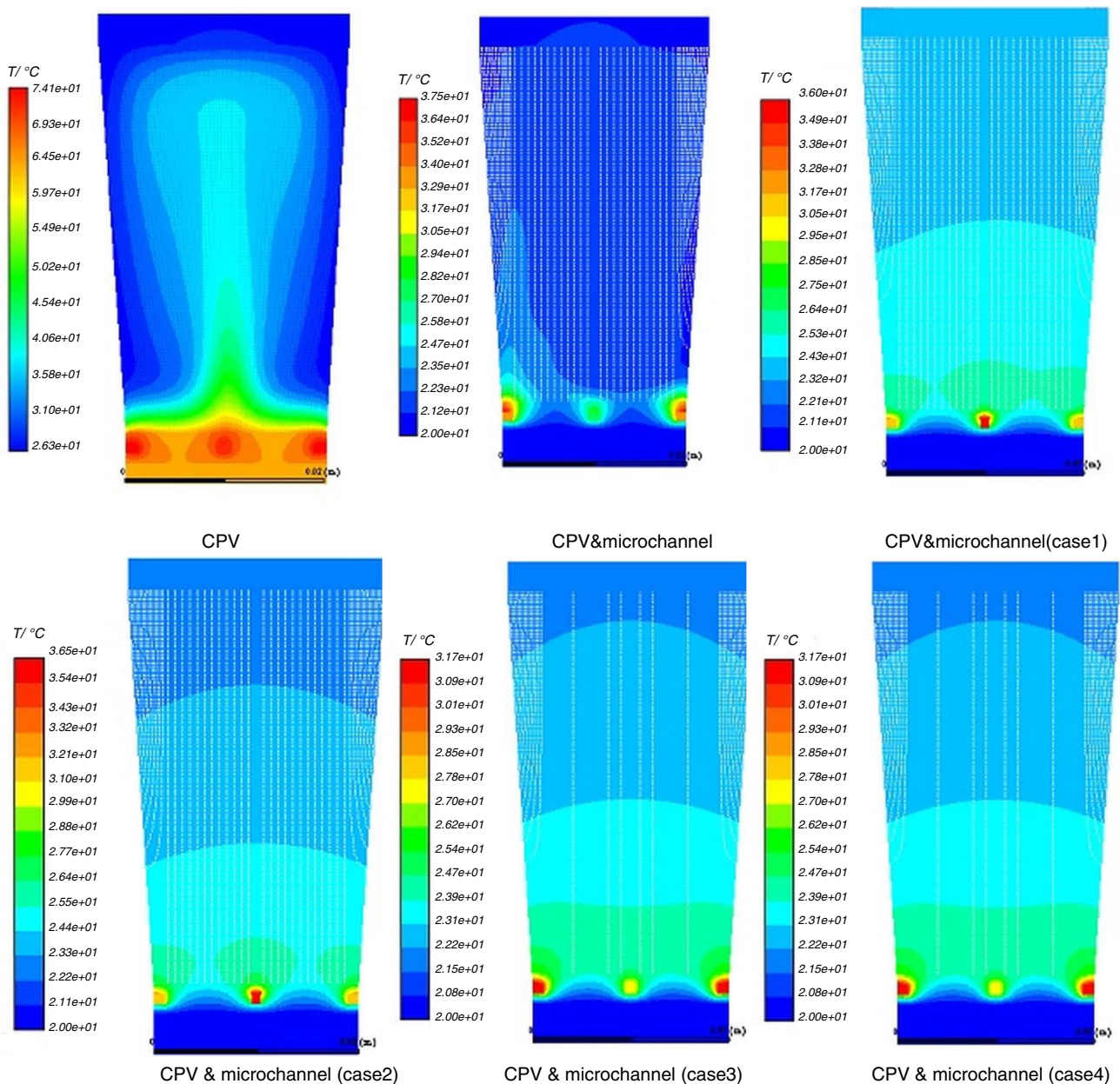


Fig. 6 Temperature contours at various cases for solar radiation = 1000 Wm^{-2} and $\text{Re} = 1000$

$\text{Re} = 100$ is higher than the other two Reynolds. The reason for this thermal behavior is the presence of porous material in the microchannel. When Reynolds is low, the fluid has a greater chance of exchanging heat in a porous medium with higher thermal conductivity. Therefore, the cooling fluid can dissipate more heat from the CPV, lower the temperature of the solar cell, and ultimately increase the electrical efficiency ratio. As the electrical efficiency ratio increases, the thermal conductivity ratio increases.

The variation of solar cell temperature, nanoparticles added to the cooling fluid can be illustrated in Fig. 9c. The conduction and convective heat transfer improve the cause

of the metal nanoparticles' dispersion in a liquid. Applying nanofluid instead of the base fluid increases the cooling capacity of the microchannel to some extent. In the microchannel with the addition of nanoparticles to the base fluid state without porous layer, and all cases 1–4, the solar cell temperature is reduced, respectively, by about 17%, 1%, and 1.4, 1.8, and 1.93% rather than to the state without nanofluid. Using nanofluid on solar cell temperature is more than the microchannel without a porous layer. With the rising volume fraction of the nanofluid, the solar cell temperature decreases, although these changes are minor.

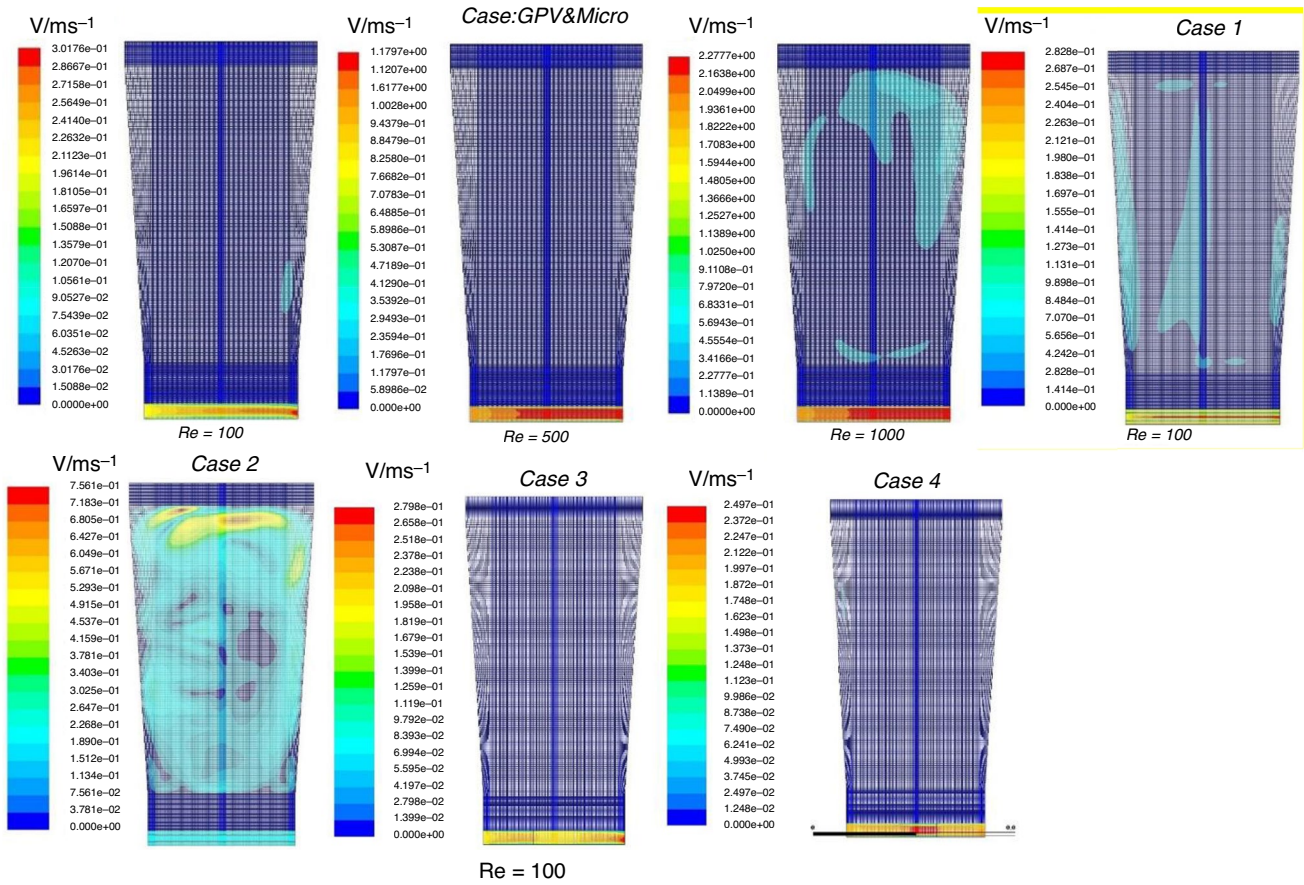


Fig. 7 Velocity contours at various cases

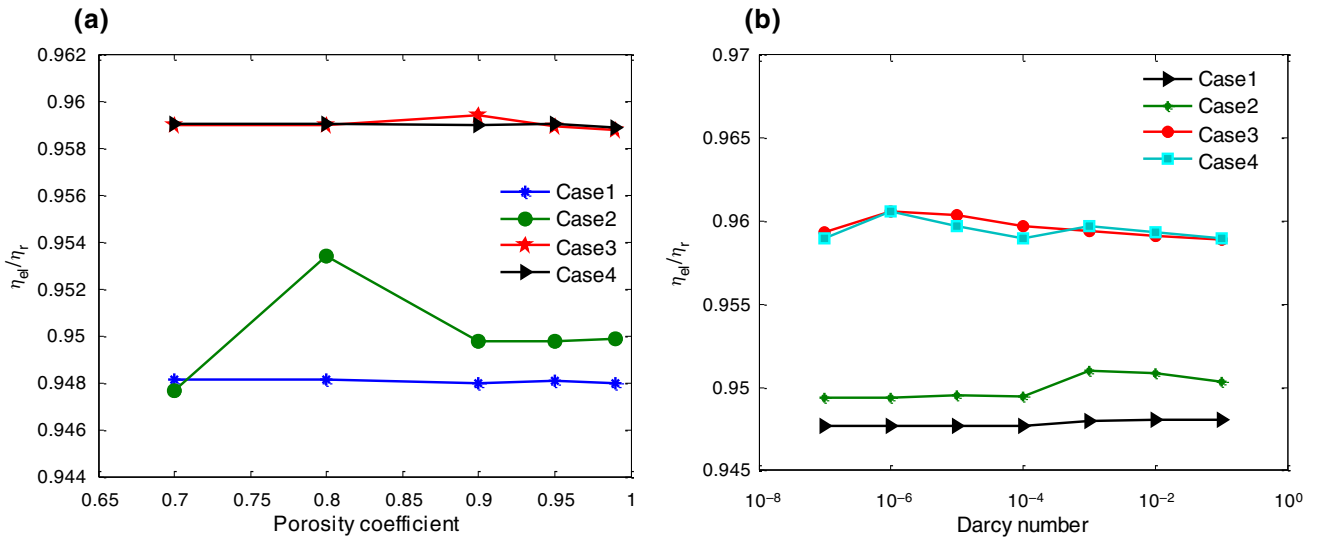


Fig. 8 Electrical efficiency ratio changes in terms of a porosity coefficient and b Darcy number

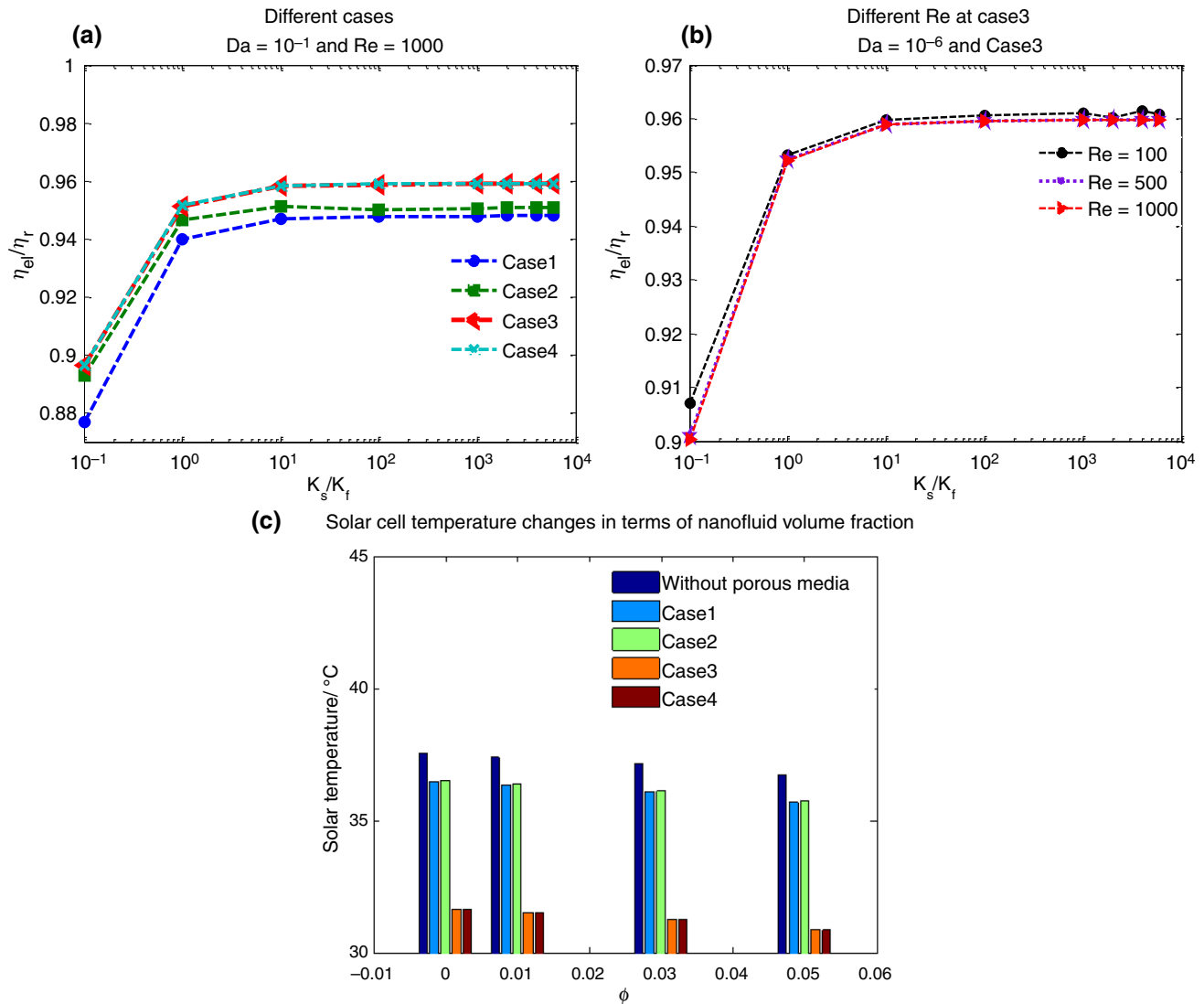


Fig. 9 Electrical efficiency ratio changes in terms of thermal conductivity ratio

To nanofluid volume, the variations of the PV/T electrical efficiency and the PV/T thermal efficiency fraction are demonstrated in Fig. 10. With increasing nanofluid volume fraction, the electrical efficiency of a solar cell increases on average is between 0.3 and 0.43%. As well, microchannel thermal efficiency improved with the rising of the nanoparticle volume fraction. This increase is on average between 4 and 7%.

One of the suggested ways to cool the CPV system is the fins usage [39]. The present study made a comparison between the CPV and microchannel system, case 3, and the CPV and Fin system (Fig. 11a). Three fins are considered with geometric parameters of the altitude and the space of 5.5 mm and 6 mm, respectively [39]. In terms of

solar radiation for both systems, the solar cell temperature changes are shown in Fig. 11b. For case 3, the porosity coefficient is 0.9, the Darcy number is 1×10^{-6} , and the Reynolds number is 1000. The results confirm that reducing the solar cell temperature by utilizing fins is 11–28%.

Using a microchannel with a porous layer with a case 3 arrangement has chilled the temperature of the solar cell by about 1–56%. In both cooling methods, the most significant decrease in solar cell temperature occurred at higher radiation intensities. The convective heat transfer is much better between the encapsulation and three complementary lenses. Thus, the cooling effect of the CPV system is improved in these areas. Temperature counters at a radiation intensity of 1000 Wm^{-2}

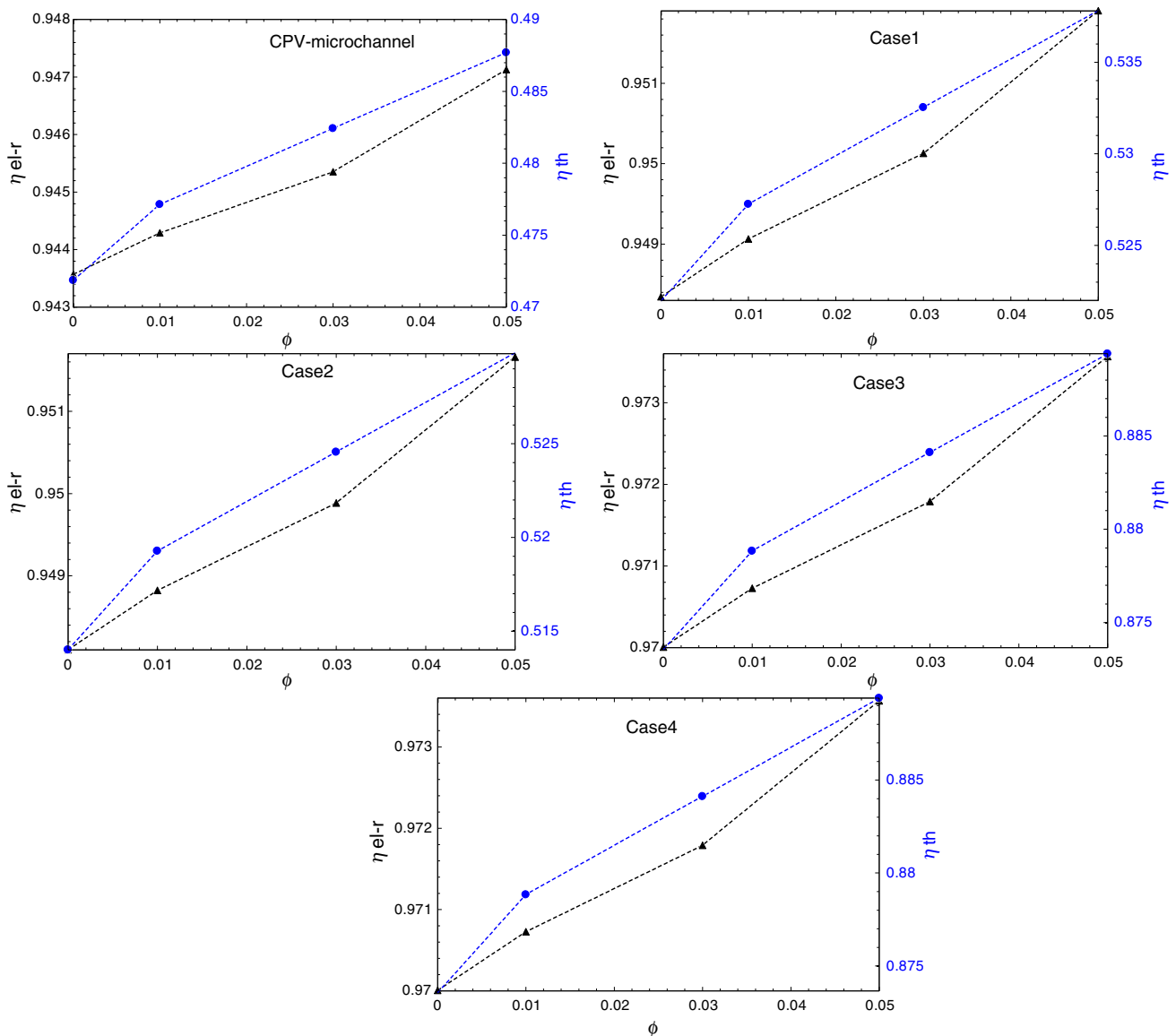


Fig. 10 Changes in the ratio of electrical efficiency and thermal efficiency in terms of nanofluid volume fraction

for both cooling systems are shown in Fig. 11c. In the case where the fin is used, the temperature changes are between 22.4 and 52.1 °C, and in case 3, the temperature changes are in the range of 20–30.8 °C. Using a CPV and microchannel system with case 3 is much more efficient than the fins cooling method. The proposed cooling method can be more effective

in expanding the electrical efficiency of the CPV system than other conventional cooling methods. The results of this research can be used in the design of solar equipment with higher efficiency. The use of methods to increase the efficiency of CPV and reduce the temperature of the solar cell has costs that can be determined according to the user's concerns [15].

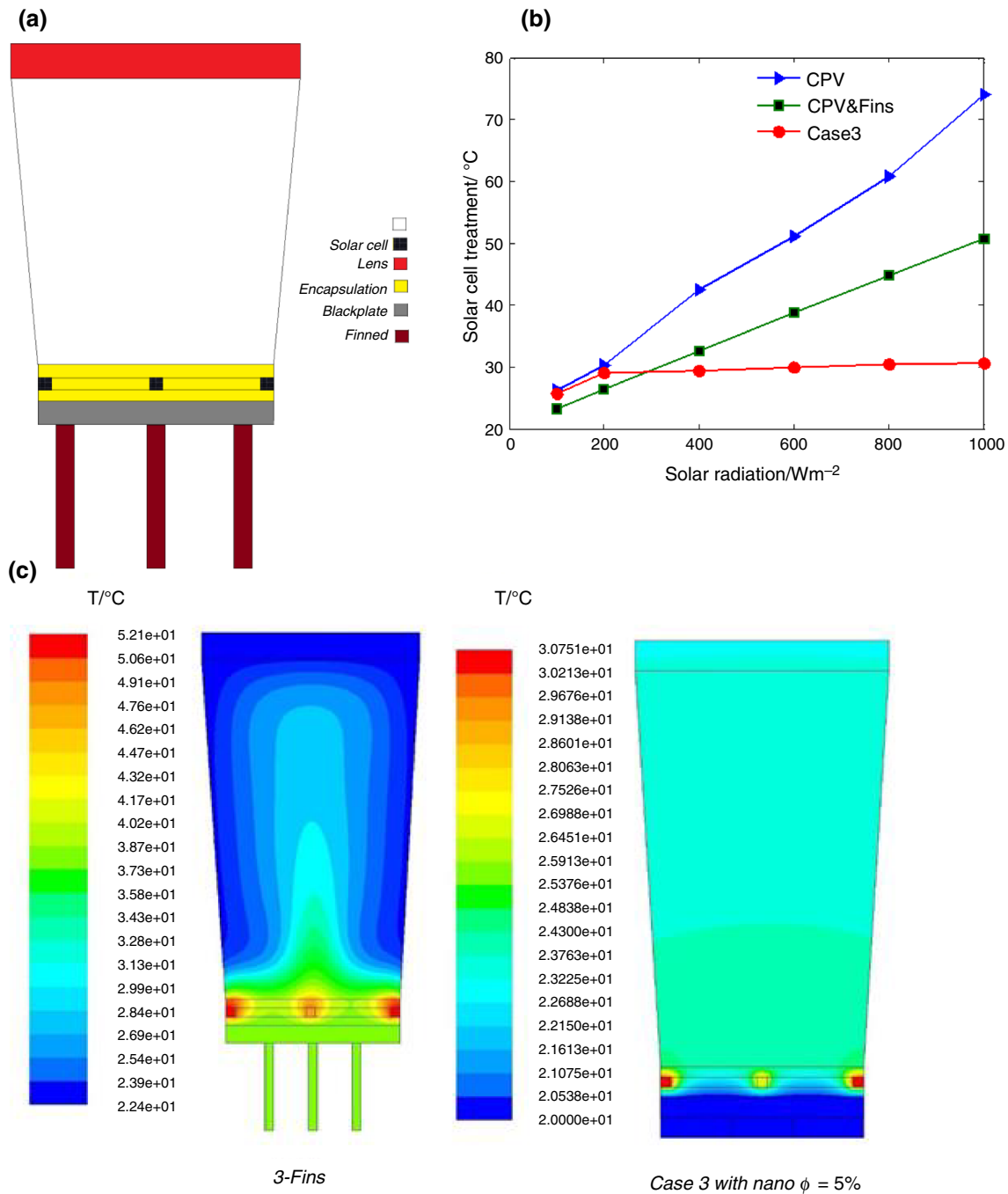


Fig.11 a A schematic of CPV and Fins, b comparison of cooling of CPV system with microchannel (case 3) and fins, c temperature contour at $1000 Wm^{-2}$ radiation intensity for case 3 and finned case

Conclusions

Increasing the temperature of the solar cell has a negative effect on the efficiency of CPVs, and due to the widespread use of CPVs, ways to improve their efficiency are significant. In this investigation, the impacts of using microchannel, the CPV system performance with porous layer arrangement in the microchannel, and nanofluid have been studied

numerically. The effect of using a porous layer in a microchannel has also been investigated for four modes of placement of a porous layer in a channel. The findings of this study are summarized below:

1. The consequences indicate that the growth of radiation intensity causes solar cell temperature increment.

2. By adding microchannels to the CPV, the solar cell temperature is significantly reduced.
3. The solar cell temperature decreases with a porous layer in the microchannel compared to the state without a porous layer. When the porous layer is blocked across the channel (case 3 and 4), more heat transfer from the CPV system is removed using the working fluid. In the range of 0.1 to 1, the thermal conductivity ratio in porous media increases the electrical CPV system efficiency by about 10%.
4. In the microchannel without porous layer and all cases 1–4, the solar cell temperature is reduced by applying nanoparticles to the base fluid. This reduction was about 17, 1, 1.%, 1.8, and 1.93% compared to the state without nanofluid. As a result, the ratio of electrical efficiency of the CPV system and thermal efficiency enhance by increasing the volume fraction of nanofluid.
5. One of the typical methods for cooling the CPV system is the use of a fin. This study made a comparison between two systems (CPV with microchannel-porous layer and CPV with fin). The CPV-micro-system's consequences confirmed that porous-layer application's solar cell temperature is tremendously more diminutive than the CPV system with fins. Eventually, the porous microchannel cooling method for CPV can replace conventional cooling methods such as fins utilization.

Author contribution SDF contributed to supervision, methodology, writing-original draft, funding acquisition, and formal analysis. MA contributed to investigation, software, visualization, resources, and writing-original draft. AZ contributed to data curation, validation, methodology, review and editing, and formal analysis. MG contributed to conceptualization, project administration, review and editing, and supervision.

Data Availability Statement The data that supports the findings of this study are available within the article.

Declaration

Conflict of interest The authors declare no conflict of interest.

References

1. Diwania S, Agrawal S, Siddiqui AS, Singh S. Photovoltaic–thermal (PV/T) technology: a comprehensive review on applications and its advancement. *Int J Energy Environ Eng*. 2020;11(1):33–54.
2. Farahani sd, Alibeigi M. Investigation of power generated from a PVT-TEG system in Iranian cities. *J Solar Energy Res*. 2020;5(4):603–616. <https://doi.org/10.22059/jser.2020.308162.1170>.
3. Chandrasekar M, Suresh S, Senthilkumar T, Ganesh Karthikeyan M. Passive cooling of standalone flat PV module with cotton wick structures. *Energy Conversion Manage*. 2018;71:43–50. <https://doi.org/10.1016/j.enconman.2013.03.012>.
4. Alshayeb MJ, Chang JD. Variations of pv panel performance installed over a vegetated roof and a conventional black roof. *Energies*. 2018;11(5):1110.
5. Odeh S. Thermal performance of dwellings with rooftop pv panels and pv/thermal collectors. *Energies*. 2018;11(7):1879.
6. Daghigh R, Ruslan MH, Sopian K. Advances in liquid based photovoltaic/thermal (PV/T) collectors. *Renew Sustain Energy Rev*. 2011;15(8):4156–70. <https://doi.org/10.1016/j.rser.2011.07.028>.
7. Abdollahi-Moghaddam M, Rejvani M, Alamdari P. Determining optimal formulations and operating conditions for Al₂O₃/water nanofluid flowing through a microchannel heat sink for cooling system purposes using statistical and optimization tools. *Thermal Sci Eng Progress*. 2018;8:517–24.
8. Bhattarai S, Oh J-H, Euh S-H, Krishna Kafle G, Hyun KD. Simulation and model validation of sheet and tube type photovoltaic thermal solar system and conventional solar collecting system in transient states. *Sol Energy Mater Sol Cells*. 2012;103:184–93. <https://doi.org/10.1016/j.solmat.2012.04.017>.
9. Hazami M, Riahi A, Mehdaoui F, Nouicer O, Farhat A. Energetic and exergetic performances analysis of a PV/T (photovoltaic thermal) solar system tested and simulated under to Tunisian (North Africa) climatic conditions. *Energy*. 2016;107:78–94. <https://doi.org/10.1016/j.energy.2016.03.134>.
10. Yazdanifard F, Ebrahimnia-Bajestan E, Ameri M. Investigating the performance of a water-based photovoltaic/thermal (PV/T) collector in laminar and turbulent flow regime. *Renewable Energy*. 2016;99:295–306. <https://doi.org/10.1016/j.renene.2016.07.004>.
11. Verma SK, Tiwari AK. Progress of nanofluid application in solar collectors: a review. *Energy Convers Manage*. 2015;100:324–46. <https://doi.org/10.1016/j.enconman.2015.04.071>.
12. Sarsam WS, Kazi SN, Badarudin A. A review of studies on using nanofluids in flat-plate solar collectors. *Sol Energy*. 2015;122:1245–65. <https://doi.org/10.1016/j.solener.2015.10.032>.
13. Alim MA, Abdin Z, Saidur R, Hepbasli A, Khairul MA, Rahim NA. Analyses of entropy generation and pressure drop for a conventional flat plate solar collector using different types of metal oxide nanofluids. *Energy Buildings*. 2013;66:289–96. <https://doi.org/10.1016/j.enbuild.2013.07.027>.
14. Chow TT, Pei G, Fong KF, Lin Z, Chan ALS, Ji J. Energy and exergy analysis of photovoltaic–thermal collector with and without glass cover. *Appl Energy*. 2009;86(3):310–6. <https://doi.org/10.1016/j.apenergy.2008.04.016>.
15. Dehghan M, Rahgozar S, Pourrajabian A, Aminy M, Halek F-S. Techno-economic perspectives of the temperature management of photovoltaic (PV) power plants: A case-study in Iran. *Sustainable Energy Technol Assess*. 2021;45: 101133. <https://doi.org/10.1016/j.seta.2021.101133>.
16. Al-Shamani AN, Sopian K, Mat S, Hasan HA, Abed AM, Ruslan MH. Experimental studies of rectangular tube absorber photovoltaic thermal collector with various types of nanofluids under the tropical climate conditions. *Energy Convers Manage*. 2016;124:528–42. <https://doi.org/10.1016/j.enconman.2016.07.052>.
17. Elmir M, Mehdaoui R, Mojtabi A. Numerical simulation of cooling a solar cell by forced convection in the presence of a nanofluid. *Energy Procedia*. 2012;18:594–603. <https://doi.org/10.1016/j.egypro.2012.05.072>.
18. Rejeb O, Sardarabadi M, Ménézo C, Passandideh-Fard M, Dhaou MH, Jemni A. Numerical and model validation of uncovered nanofluid sheet and tube type photovoltaic thermal solar system. *Energy Convers Manage*. 2016;110:367–77. <https://doi.org/10.1016/j.enconman.2015.11.063>.
19. Sardarabadi M, Passandideh-Fard M. Experimental and numerical study of metal-oxides/water nanofluids as coolant in

- photovoltaic thermal systems (PVT). *Sol Energy Mater Sol Cells*. 2016;157:533–42. <https://doi.org/10.1016/j.solmat.2016.07.008>.
20. Sharma S, Micheli L, Chang W, Tahir AA, Reddy KS, Mallick TK. Nano-enhanced phase change material for thermal management of BICPV. *Appl Energy*. 2017;208:719–33. <https://doi.org/10.1016/j.apenergy.2017.09.076>.
 21. Dehghan M, Vajedi H, Daneshipour M, Pourrajabian A, Rahgozar S, Iliis GG. Pumping power and heat transfer rate of converging microchannel heat sinks: errors associated with the temperature dependency of nanofluids. *J Therm Anal Calorim*. 2020;140(3):1267–75. <https://doi.org/10.1007/s10973-019-09020-y>.
 22. Dehghan M, Daneshipour M, Valipour MS. Nanofluids and converging flow passages: A synergetic conjugate-heat-transfer enhancement of micro heat sinks. *Int Commun Heat Mass Transfer*. 2018;97:72–7. <https://doi.org/10.1016/j.icheatmasstransfer.2018.03.022>.
 23. Rabie R, Emam M, Ookawara S, Ahmed M. Thermal management of concentrator photovoltaic systems using new configurations of phase change material heat sinks. *Sol Energy*. 2019;183:632–52. <https://doi.org/10.1016/j.solener.2019.03.061>.
 24. Al Siyabi I, Shanks K, Mallick T, Sundaram S. Indoor and outdoor characterization of concentrating photovoltaic attached to multi-layered microchannel heat sink. *Sol Energy*. 2020;202:55–72. <https://doi.org/10.1016/j.solener.2020.03.101>.
 25. Abo-Zahhad EM, Ookawara S, Esmail MFC, El-Shazly AH, Elkady MF, Radwan A. Thermal management of high concentrator solar cell using new designs of stepwise varying width microchannel cooling scheme. *Appl Therm Eng*. 2020;172: 115124. <https://doi.org/10.1016/j.applthermaleng.2020.115124>.
 26. Sarafraz M, Safaei MR, Leon AS, Tlili I, Alkanhal TA, Tian Z, et al. Experimental investigation on thermal performance of a PV/T-PCM (photovoltaic/thermal) system cooling with a PCM and nanofluid. *Energies*. 2019;12(13):2572.
 27. Sardarabadi M, Passandideh-Fard M, Maghrebi M-J, Ghazikhani M. Experimental study of using both ZnO/water nanofluid and phase change material (PCM) in photovoltaic thermal systems. *Sol Energy Mater Sol Cells*. 2017;161:62–9.
 28. Shahsavari A, Khanmohammadi S, Karimipour A, Goodarzi M. A novel comprehensive experimental study concerned synthesizes and prepare liquid paraffin-Fe₃O₄ mixture to develop models for both thermal conductivity & viscosity: a new approach of GMDH type of neural network. *Int J Heat Mass Transf*. 2019;131:432–41.
 29. Nasef HA, Nada SA, Hassan H. Integrative passive and active cooling system using PCM and nanofluid for thermal regulation of concentrated photovoltaic solar cells. *Energy Convers Manage*. 2019;199: 112065. <https://doi.org/10.1016/j.enconman.2019.112065>.
 30. Arani AAA, Akbari OA, Safaei MR, Marzban A, Alrashed AA, Ahmadi GR, et al. Heat transfer improvement of water/single-wall carbon nanotubes (SWCNT) nanofluid in a novel design of a truncated double-layered microchannel heat sink. *Int J Heat Mass Transf*. 2017;113:780–95.
 31. Haghghi SS, Goshayeshi H, Safaei MR. Natural convection heat transfer enhancement in new designs of plate-fin based heat sinks. *Int J Heat Mass Transf*. 2018;125:640–7.
 32. Dadsetani R, Sheikhzadeh GA, Hajmohammadi MR, Safaei MR. Introduce a novel configuration of microchannel and high-conductivity inserts for cooling of disc-shaped electronic components. *Int J Numer Methods Heat Fluid Flow*. 2019.
 33. Jalali E, Ali Akbari O, Sarafraz M, Abbas T, Safaei MR. Heat transfer of oil/MWCNT nanofluid jet injection inside a rectangular microchannel. *Symmetry*. 2019;11(6):757.
 34. Alazwari MA, Safaei MR. Combination effect of Baffle arrangement and hybrid nanofluid on thermal performance of a shell and tube heat exchanger using 3-D Homogeneous mixture model. *Mathematics*. 2021;9(8):881.
 35. Anitha S, Safaei MR, Rajeswari S, Pichumani M. Thermal and energy management prospects of γ -AlOOH hybrid nanofluids for the application of sustainable heat exchanger systems. *J Thermal Anal Calorimetry*. 2021:1–17. <https://doi.org/10.1007/s10973-021-10996-9>.
 36. Ho C, Hsu S-T, Yang T-F, Chen B-L, Rashidi S, Yan W-M. Cooling performance of mini-channel heat sink with water-based nano-PCM emulsion-An experimental study. *Int J Thermal Sci*. 2021;164:106903.
 37. Safaei MR, Goshayeshi HR, Chaer I. Solar still efficiency enhancement by using graphene oxide/paraffin nano-PCM. *Energies*. 2019;12(10):2002.
 38. Mallick TK, Eames PC, Norton B. Using air flow to alleviate temperature elevation in solar cells within asymmetric compound parabolic concentrators. *Sol Energy*. 2007;81(2):173–84. <https://doi.org/10.1016/j.solener.2006.04.003>.
 39. Natarajan SK, Mallick TK, Katz M, Weingaertner S. Numerical investigations of solar cell temperature for photovoltaic concentrator system with and without passive cooling arrangements. *Int J Therm Sci*. 2011;50(12):2514–21. <https://doi.org/10.1016/j.ijthermalsci.2011.06.014>.
 40. Alibeigi M, Farahani SD. Effect of porous medium positioning on heat transfer of micro-channel with jet. *Int J Eng*. 2020;33(10):2057–64. <https://doi.org/10.5829/ije.2020.33.10a.24>.
 41. Nield DA, Bejan A. Convection in porous media. Springer; 2006.
 42. Hemmat Esfe M, Esfandeh S, Hosseinzadeh E. Nanofluid flooding in a randomized heterogeneous porous media and investigating the effect of capillary pressure and diffusion on oil recovery factor. *J Mol Liq*. 2020;320: 113646. <https://doi.org/10.1016/j.molliq.2020.113646>.
 43. Hariri S, Mokhtari M, Gerdroodbary MB, Fallah K. Numerical investigation of the heat transfer of a ferrofluid inside a tube in the presence of a non-uniform magnetic field. *Euro Phys J Plus*. 2017;132(2):65. <https://doi.org/10.1140/epjp/i2017-11324-1>.
 44. Ho C-J, Wei L, Li Z. An experimental investigation of forced convective cooling performance of a microchannel heat sink with Al₂O₃/water nanofluid. *Appl Therm Eng*. 2010;30(2–3):96–103.
 45. Silva RA, de Lemos MJ. Numerical analysis of the stress jump interface condition for laminar flow over a porous layer. *Numer Heat Transfer: A Applications*. 2003;43(6):603–17.
 46. Sopian K, Alghoul MA, Alfegi EM, Sulaiman MY, Musa EA. Evaluation of thermal efficiency of double-pass solar collector with porous–nonporous media. *Renewable Energy*. 2009;34(3):640–5. <https://doi.org/10.1016/j.renene.2008.05.027>.
 47. Baig H, Heasman KC, Mallick TK. Non-uniform illumination in concentrating solar cells. *Renew Sustain Energy Rev*. 2012;16(8):5890–909.
 48. Al-Showany EFA. The impact of the environmental condition on the performance of the photovoltaic cell. *Am J Energy Eng*. 2016;4(1):1–7.
 49. Evans D. Simplified method for predicting photovoltaic array output. *Sol Energy*. 1981;27(6):555–60.
 50. Farahani SD, Sarlak MA, Alibeigi M. Thermal analysis of PVT-HEX system: Electricity Efficiency and Air Conditioning System. *Journal of Solar Energy Research*. 2021;6(1):625–33.
 51. Incropera FP, Lavine AS, Bergman TL, DeWitt DP. Fundamentals of heat and mass transfer. Wiley; 2007.
 52. Du B, Hu E, Kolhe M. Performance analysis of water cooled concentrated photovoltaic (CPV) system. *Renew Sustain Energy Rev*. 2012;16(9):6732–6.

Publisher's Note Springer Nature remains neutral with regard to jurisdictional claims in published maps and institutional affiliations.